15TH IEA HEAT PUMP CONFERENCE
MAY 26–29, 2026 | HOFBURG
VIENNA 2026
DECARBONISATION THROUGH INNOVATION

Impact of local heat pump characteristics on the performance of a CO_2-based thermal network

Sepehr Gholamrezaie[a,*], Massimo Cimmino[a], Parham Eslami-Nejad[a,b]

[a]Department of Mechanical Engineering, Polytechnique Montréal, Montréal, Québec, Canada
[b]Vitalis equipment technology, Kelowna, British Columbia, Canada

Abstract

CO_2-based thermal networks (CO_2TN) connected to local heat pumps (LHPs) offer a promising approach for thermal energy distribution in buildings. These systems circulate two-phase CO_2 at near-indoor (room) temperature through a single pipe (the CO_2 loop), which serves as the source side for LHPs connected in series. This configuration enables heat recovery between zones and as it operates at an almost constant temperature near indoor temperature, it reduces both heat losses through pipes and insulation requirements. Previous studies have shown that LHP's performance has a significant impact on the overall system performance. Standard heat pumps, typically designed for higher temperature difference between source and sink (temperature lift), operate quite well for conventional outdoor temperature ranges. However, they may not operate optimally when the source side is near room temperature and the required temperature lift is relatively small. This study evaluates how local heat pump performance characteristics influence the system-wide efficiency of a representative CO_2TN. The network includes a CO_2 circulation system, LHPs, and an outdoor unit that exchanges heat between the CO_2TN and the environment. A detailed simulation model is developed, incorporating all major system components: the circulation compressor, internal heat exchanger, outdoor-side heat exchangers (gas cooler, condenser, and evaporator), and local heat pumps. The base case is modeled using a commercially available LHP unit that has been modified at CanmetENERGY (Varennes, Canada) to integrate with the CO_2 loop. To explore potential system improvements, additional simulations are conducted using idealized performance curves that approximate thermodynamically optimized cycles. Based on the presented simulation results, avenues to improve the efficiency of the system by better selection of the heat pump units are identified.

Keywords: CO_2 thermal network; Low-lift heat pump; Building heating and cooling; Control

1. Introduction

CO_2 Thermal Network (CO_2TN) is a building-scale cascade system proposed by Eslami-Nejad et al. [1]. It arranges a central reversible vapor-compression cycle using CO_2 (R744) to circulate a two-phase CO_2 stream at near-room-temperature through a single-pipe loop that serves multiple packaged local heat pumps (LHPs). We refer to the central plant as the RVCC (reversible vapor-compression cycle) and to the circulating line at the source of the LHPs as the "CO_2-loop." The loop intentionally operates close to room temperature so that the source side experienced by all LHPs is nearly isothermal; the loop fluid carries heat primarily through phase change, so relatively small mass flow rates and compact pipe diameters are sufficient. LHPs are connected in series along the single pipe. Each LHP has its own sealed refrigerant circuit sized for the zone it serves. When a LHP runs in cooling, it rejects heat into the two-phase CO_2 stream and increases the CO_2 quality (vapor mass fraction); when a LHP runs in heating, it absorbs heat from the loop and decreases the CO_2 quality. This counter-balancing behavior enables internal heat recovery: heat rejected upstream can be re-used downstream without changing the loop temperature. Fig. 1 illustrates the system on a pressure-enthalpy (p-h) diagram. The cycle shows the RVCC preparing CO_2 to enter the CO_2-loop at point 5, after which it flows through the series of LHPs.

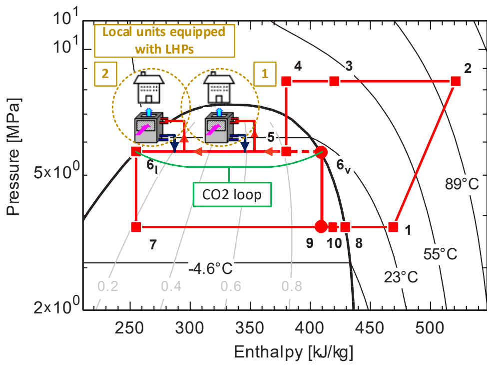

Figure 1. CO_2TN Overview

The concept has been demonstrated experimentally with a pilot-scale prototype built at CanmetENERGY–Varennes and presented by Bastani and Gholamrezaie [2]. In brief, the prototype comprises a CO_2 RVCC (compressor, gas cooler, internal heat exchangers, receiver/accumulator, expansion/control valve set) feeding a stainless-steel single-pipe loop and instrumented with pressure, temperature and mass-flow sensors. Three packaged LHPs are used that can be set in all-cooling or all-heating and mixed arrangements to emulate diverse multi-zone demands and simultaneous operation. This prototype established feasibility, provided high-resolution datasets for model validation, and established the reference architecture used in the present work.

Using the prototype data as ground truth, we developed and validated a detailed model of the CO_2TN [3], including component-level representations (compressor maps, gas cooler and CO_2-CO_2/CO_2-water heat exchangers, internal heat exchangers) and a building-side representation of LHPs and zone loads. Validation was performed both at component level and system level against the prototype. The model reproduces the loop thermodynamics (pressure, enthalpy evolution, and quality path) and the RVCC operating envelope across the heating and cooling modes used in the experiments.

On supervisory control, our 2022 study [4] introduced a minimum-mass-flow strategy tailored to the single-pipe, two-phase CO_2 loop. Based on cumulative heat exchange along the loop (evaluated at the outlet of each heat pump), a loop entry enthalpy can be evaluated to allow the smallest possible CO_2 mass flow that still maintains the loop within two-phase from start to end. The plant setpoints are selected to deliver that target within equipment limits. As our next study in 2024 revealed [5], we found that operating strictly at minimum mass flow with a saturated loop outlet can impair performance compared to the optimum operation. In practice, the overall efficiency varies with both the loop circulation and the chosen pressures: the maximum system efficiency often occurs away from the minimum-flow point, and allowing a small amount of superheat or sub-cool along the loop and at its outlet can further reduce circulation and compression work with only a slight performance penalty at LHPs. This motivates a relaxed-constraint supervisory approach that treats circulation and pressures as free decision variables rather than simply aiming for minimum CO_2 mass flow in the loop.

For the system to perform optimally, energy consumption of both the RVCC and the LHPs are equally important and they must operate efficiently. In our study, the key linkage between the RVCC and the LHPs is the source-side temperature seen by the LHPs, which the RVCC indirectly controls through the CO_2 loop pressure and mass flow it generates. The RVCC can provide this source temperature only within a workable range, bounded by equipment limits and operation stability. This raises a research question: how does LHP performance impact the overall efficiency of the system?

The efficiency of each LHP depends strongly on its source temperature. For a given building demand, a higher source temperature lowers the internal temperature lift—the difference between the evaporation and condensation temperatures within the heat pump—and thereby increases the coefficient of performance (COP). In practice, conventional commercial units are optimized for temperature lifts of 30 to 60 K, which limits their potential for efficiency improvement when operating at lower temperature lift conditions such as those provided by the CO_2 thermal network. In contrast, low-temperature-lift heat pumps, designed specifically for small lifts of 10 to 30 K, can achieve substantially higher performance. Gasser et al. [6] developed and experimentally tested two such prototypes: one using a reciprocating compressor and the other employing a small-scale, oil-free turbo compressor. The study demonstrated that at a lift of 20 K, the reciprocating unit achieved a heating COP above 9, while the turbo-compressor variant reached COP values of up to 14 for lifts below 15 K, corresponding to a nearly constant Carnot efficiency of about 60%. These results confirm the significant potential of low-lift systems when the temperature difference between the source and the sink is minimized.

Consistent with our previous prototype [2] and modeling work [3], the baseline LHPs are modified commercial units integrated into the CO_2TN. To explore the impact of different LHPs, we extend that baseline with two low-lift concepts from the literature: (1) a reciprocating-compressor heat pump optimized for small lifts and (2) an oil-free, small-scale turbo-compressor heat pump designed to maintain a high, relatively constant fraction of Carnot efficiency across 10 to 30 K lifts. Because the overall system performance depends on both the RVCC and the LHPs, it is not evident a priori how an increase in LHP COP will translate into system-level COP. In particular, the COPs of the LHPs depend on their source-side temperature, which is set by the CO_2 loop and therefore controlled by the RVCC; any change in LHP performance can thus modify the optimal loop pressure, mass flow rate, and operating regime of the circulation compressor. This study implements those two LHP models alongside the commercial baseline within the validated CO_2TN framework and compares the overall COP of the system for a five-zone case under identical RVCC and control settings.

2. System overview

The system comprises three main sections. First, a reversible vapor-compression cycle (RVCC) circulates CO_2, exchanges heat at the outdoor unit (absorbing or rejecting as needed), and supplies the CO_2 loop at the required pressure and temperature. Second, the outdoor unit is, in this study, a secondary hydronic loop coupled to geothermal boreholes. Third, packaged local heat pumps (LHPs) connect in series to the CO_2 loop and condition the individual zones. Fig. 2 shows the process flow diagram of the system.

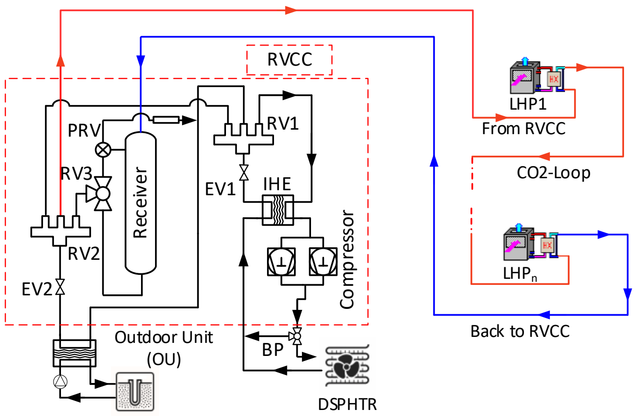

Figure 2. System process flow diagram

Fig. 3 presents the CO_2 thermal network (CO_2TN) on a pressure-enthalpy chart and anchors the description of both operating regimes. The RVCC is a reversible vapor-compression circulation unit comprising two compressors (one variable-speed and one fixed-speed), a desuperheater, an outdoor heat exchanger whose role switches with the mode, an internal heat exchanger, a receiver, and expansion/pressure-regulation valves. A single-pipe CO_2 loop carries a near-room temperature, two-phase CO_2 that serves the source side of packaged local heat pumps (LHPs) connected in series. Each LHP conditions its zone and exchanges heat with the loop: in cooling, it rejects heat to the loop; in heating, it extracts heat from it.

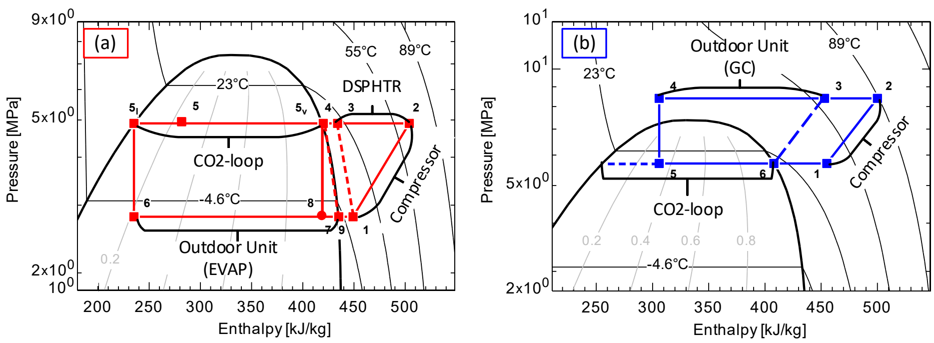

Figure 3. (a) heating dominant mode; (b) cooling dominant mode

In heating-dominant operation (Fig. 3a, red), the cycle begins at the compressor inlet (point 1) and proceeds to the discharge state (point 2). The discharge then passes through the desuperheater, where sensible heat is removed (points 2 to 3). Next, the internal heat exchanger transfers heat from the high-pressure side (points 3 to 4) to the suction side (points 9 to 1), ensuring a superheat of +10 °C at the compressor inlet. At point 4, the CO_2 enters the CO_2 loop and circulates through the source side of the LHPs. As the fluid flows through the series of LHPs (points 4 to 5), zones requiring heating extract heat from the loop, while any cooling zones reject heat. This combined effect alters the vapor fraction along the pipe until the stream exits the building loop at point 5. The returning flow accumulates in the receiver, where vapor (point 5v) and liquid (point 5l) phases separate. The liquid portion expands in an isenthalpic process from point 5 to 6 down to a pressure suitable to exchange heat with the outdoor unit. From point 6 to 7, the CO_2 passes through the outdoor unit, which operates as an evaporator (EVAP) absorbing heat from the external geothermal source. Finally, the vapor stream passes through the suction side of the internal heat exchanger (point 9), where the desired +10 °C superheat is maintained before returning to the compressor inlet (point 1), thus completing the heating-dominant cycle.

In cooling-dominant operation (Fig. 3b, blue), the compressor again raises the CO_2 pressure and temperature from suction (point 1) to discharge (point 2). Between points 2 and 3, the internal heat exchanger provides heat to the suction side, ensuring sufficient superheat at the compressor inlet. From points 3 to 4, the outdoor unit now rejects heat to the environment, acting as a gas cooler (GC) in transcritical operation or as a condenser (COND) in subcritical conditions. At the gas cooler outlet (point 4), the CO_2 expands through the expansion valve to the inlet of the CO_2 loop, where it then flows on the source side of the LHPs (point 5). As the fluid progresses through the LHPs (points 5 to 6), zones operating in cooling reject heat to the loop and increase its vapor fraction, while any heating zones absorb heat from the stream. The return flow then passes through the internal heat exchanger (point 6) and suction line before reaching the compressor inlet (point 1), completing the cooling-dominant cycle. The same hardware supports both operating regimes; the distinction lies in the aggregate building demand and the role of the outdoor unit. When the combined effect of the active LHPs adds heat to the loop, the plant operates in cooling-dominant mode with the outdoor unit rejecting heat. When the net effect removes heat from the loop, the plant operates in heating-dominant mode with the outdoor unit absorbing heat. Either regime can operate in subcritical or transcritical conditions depending on the selected pressures and the external environment.

3. Case study: 5-zone building

We implemented the CO_2TN on a small office building in Montreal, Canada to evaluate its performance. The floor plan comprises five thermal zones—four perimeter zones (West, South, East, North) surrounding a Core zone. Annual zone loads follow Tamasauskas et al. [7] and are summarized in Table 1. H and C denote heating and cooling, respectively. With respect to this case study, we sized and implemented the system.

Table 1. Load characteristics

Zone	West		South		East		North		Core	
	H	C	H	C	H	C	H	C	H	C
Total Demand [kWh]	2050	2813	2198	5122	1849	2773	3020	3732	1014	6070
Peak Load [kW]	3.3	4.2	5.1	4.4	3.3	3.8	5.3	3.4	4.2	3.7
Total Demand Duration [h]	3692	2482	2263	4074	3352	2816	2585	3722	1267	4885

4. Modelling approach

The system is modelled component-by-component using the same compressor, heat exchanger and loop models that were developed and experimentally validated in Gholamrezaie et al. [3]. Only the main features are summarized here; elements that differ from the previous study (dual compressors and the local heat pump archetypes) are described in more detail. The main components of the system are two semi-hermetic reciprocating compressors in parallel (one variable-speed and one fixed-speed), a desuperheater (DSPHTR) in line for heating mode and bypassed in cooling mode, an internal heat exchanger (IHE), LHPs, and the CO_2–water plate heat exchanger outdoor unit connected to a geothermal borefield.

In this study, pressure drops in pipes and across components are neglected and all expansion valves are modelled as isenthalpic throttling devices, consistent with the validated model.

4.1. Compressor

Compressors are modelled with the third-order polynomial mapping originally developed and validated in Gholamrezaie et al. [3]. This model extends the AHRI 540 approach to a three-variable polynomial fitted to manufacturer data for a transcritical semi-hermetic reciprocating CO_2 compressor. The inputs are suction pressure P_{suc}, discharge pressure P_{dis}, and compressor speed S (Hz); the outputs are the compressor power input $\dot{W}_{comp}$ and the CO_2 mass flow rate $\dot{m}_{CO_2}$. Both quantities are expressed through a general third-order polynomial in the three variables:

$$X = f(P_{suc}, P_{dis}, S) \quad (1)$$

where X represents either $\dot{W}_{comp}$ or $\dot{m}_{CO_2}$ using two distinct sets of coefficients. The polynomial contains up to cubic terms and cross-terms in P_{suc}, P_{dis} and S; its 22 coefficients were obtained by regression on 100 operating points covering 30–75 Hz, 2–5.8 MPa suction pressure and 6–12 MPa discharge pressure and presented in Gholamrezaie et al. [3].

The discharge state is then obtained from the energy balance as follows:

$$\dot{W}_{comp} = \dot{m}_{CO_2}.(h_{dis} - h_{suc}) \quad (2)$$

where h_{dis} and h_{suc} are discharge and suction enthalpies, respectively. In the previous study, a single compressor was used. In the present work, two identical compressors are installed in parallel to increase turndown and part-load performance. Using similarity laws, each compressor is modeled as a half-size version of the reference machine: the same polynomial form is retained, but the power and mass-flow maps are scaled by a factor of 1/2.

4.2. Heat exchangers

Two types of plate heat exchangers are used in the system: CO_2-to-CO_2 plate heat exchanger used as the internal heat exchanger (IHE), and CO_2-to-water plate heat exchangers used as the desuperheater (DSPHTR), gas cooler (GC) or condenser (COND), and evaporator (EVAP).

4.2.1. CO_2 –CO_2 plate heat exchangers (Internal heat exchanger)

The IHE is treated as an ideal counter-flow heat exchanger with no external losses. It transfers heat from the discharge line to the suction line until the required superheat at compressor inlet is obtained. Consistent with the previous model, it is represented as a perfect heat exchanger with a fixed pinch constraint, such that the enthalpy at the compressor suction is adjusted to provide the target superheat while conserving energy between the hot and cold sides.

4.2.2. Water–CO_2 plate heat exchangers (DSPHTR, GC/COND, EVAP)

The water-to-CO_2 plate heat exchanger model developed in Gholamrezaie et al. [3] is reused here for the DSPHTR, GC/COND and EVAP. Water glycol 30% mixture flows in counter-flow to CO_2. Depending on the thermodynamic region of CO_2, three different models are used. All plate heat exchangers are assumed adiabatic with negligible pressure loss on both CO_2 and water–glycol sides, as in the validation work.

In the transcritical/superheated region, the thermophysical properties of CO_2 vary rapidly and the heat exchanger is discretized into *n* cells along the flow direction. In each cell, the water–glycol properties are assumed constant and equal to their value at the outlet of the cell, while CO_2 properties are evaluated with CoolProp. Segment-wise energy balances are solved with convective heat transfer coefficients obtained from standard correlations for turbulent water–glycol flow and for superheated/supercritical CO_2. This discretized model captures the strong variation of CO_2 properties near the critical region and was previously validated against experimental data in Gholamrezaie et al. [3].

When the discharge pressure is below the critical point, the outdoor heat exchanger operates as a condenser. It is modelled with a moving-boundary approach that divides the plate into three zones (superheated, two-phase and sub-cooled). Each zone is treated as a lumped element, and the moving interfaces between zones are determined from energy balances in each region. This provides a computationally efficient representation of phase change while retaining sensitivity to inlet conditions and mass flow rate.

When the outdoor unit operates as an evaporator, an $\varepsilon - NTU$ method is used. The overall heat transfer coefficient and area are taken from the validated model, and effectiveness is evaluated as a function of the number of transfer units and capacity-rate ratio.

4.3. CO_2 loop

The single-pipe CO_2 loop is modelled as a near-isothermal two-phase stream that passes sequentially by the LHP interfaces. Rather than resolving detailed pipe-side heat transfer, the model tracks the enthalpy of the loop at the inlet and outlet of each LHP. At a given loop pressure, the saturation temperature is fixed, so the local CO_2 quality changes as zones reject or absorb heat. The loop pressure is controlled and assumed uniform along the loop. This simplification is justified because loop pressure losses are small relative to the compressor pressure rise and cause only minor shifts in two-phase saturation temperature, so their impact on LHP performance is negligible.The loop enthalpy after each LHP in the sequence is obtained from an energy balance, where the LHP capacity and power consumption are used to determine the CO_2 outlet enthalpy as follows:

In heating mode:

$$\dot{Q}_{HP,H,i} - \dot{W}_{HP,i} = \dot{m}_{CO_2}.(h_{HP,in,i} - h_{HP,out,i}) \tag{3}$$

In cooling mode:

$$\dot{Q}_{HP,C,i} + \dot{W}_{HP,i} = \dot{m}_{CO_2}.(h_{HP,out,i} - h_{HP,in,i}) \tag{4}$$

where $\dot{Q}_{HP,H/C,i}$, and $\dot{W}_{HP,i}$ are the heating/cooling capacity and power of the *i-th* LHP, and $h_{HP,in,i}$, $h_{HP,out,i}$ are the CO_2 enthalpies at its inlet and outlet.

4.4. Ground heat exchanger and borefield sizing

On the source/sink side, the RVCC exchanges heat with the ground via a CO_2–water plate heat exchanger connected to a secondary hydronic loop circulating 30% water-glycol mixture (the outdoor unit). The vertical borefield simulated with TRNSYS Type 557a, which accounts for borehole thermal resistance and both short- and long-term ground response. Undisturbed ground temperature (10.5 ℃), thermal conductivity ($2.65\ W/m-k$) and diffusivity ($0.08\ m^2/day$) are taken from the literature [8-9]. The borefield size (number and length of boreholes) is determined with the Alternative ASHRAE sizing method [10] and then kept fixed for all dynamic simulations. During the simulations, the pump in the secondary loop is controlled to maintain the desired temperature approach between the borefield outlet and CO_2 inlet to the outdoor unit plate heat exchanger. This ensures that the outdoor unit can supply (or absorb) the total thermal load required by the CO_2 thermal network while keeping the borehole outlet temperature within a target range (typically 5–25 °C). Table 2 is the result of borehole sizing for the case study introduced earlier.

Table 2. Borefield sizing

Borefield layout	Value
Layout $N_{bx} \times N_{by}$	5 × 1
Bore spacing s	7.5 m
Per-bore depth H	127 m
Total length L_{tot}	635 m

4.5. Local heat pump (LHP)

Each LHP is represented by compact performance maps that link its heating/cooling capacity and power consumption to the source temperature provided by the CO_2 loop and to the internal temperature lift between source and sink. Three different LHP archetypes are considered in this study: a baseline modified "commercial" unit used in the CanmetENERGY CO_2TN prototype [2], a low-lift reciprocating-compressor unit, and a low-lift turbo-compressor unit. All three archetypes are normalized to provide the same nominal zone load at a common reference point, so that system-level comparisons reflect differences in intrinsic HP performance rather than sizing.

4.5.1. Modified commercial local heat pump

For the baseline unit used and modified in the prototype, we reuse the identified COP surfaces and implementation from the validated model [3]. Experimental data from modified CO_2-to-air HPs tested at CanmetENERGY were regressed as functions of the CO_2 loop temperature (T_{loop}) for both heating and cooling modes:

$$COP_{HP,C} = -0.08.T_{loop} + 5.04 \tag{5}$$

$$COP_{HP,H} = -0.05.T_{loop} + 2.77 \tag{6}$$

where T_{loop} is in °C.

For a given mode j (heating or cooling), the electrical power is obtained from the following relation:

$$\dot{W}_{HP,j} = \frac{\dot{Q}_{HP,j}}{COP_{HP,j}} \tag{7}$$

4.5.2. Low-lift reciprocating-compressor local heat pump

The low-lift reciprocating LHP archetype is based on the prototype described by Gasser et al. [6], in which a positive-displacement reciprocating compressor uses propane (R290) as refrigerant and is optimized for operation with small internal temperature lifts. The prototype is intended for applications with relatively high source temperatures (e.g., deep geothermal or ambient-assisted sources) and low-temperature heating distribution, so that the internal lift typically lies in the range of about 15 to 30 K. In this context, the internal temperature lift is defined as the difference between the condensation and evaporation saturation temperatures of the refrigerant inside the cycle as follows:

$$\Delta T_{lift} = T_{cond} - T_{evap} \tag{8}$$

Here T_{evap}, and T_{cond} (in K) are the saturation temperatures at the evaporator and condenser pressure levels respectively. In the CO_2TN, depending on the operating mode, the evaporation temperature of the local R290 LHP in heating mode is tied to the CO_2 loop saturation temperature, while the condensation temperature follows the supply temperature required by the zone. In cooling mode, the condensation temperature of the LHP is tied to the CO_2 loop, whereas the evaporation temperature follows the supply temperature required for cooling. For the reciprocating low-lift archetype, the COP is written as a Carnot COP multiplied by a lift-dependent Carnot efficiency. The real COPs of the low-lift reciprocating unit are then expressed as:

$$COP_{HP,C} = \eta_{rec}.\frac{T_{evap}}{\Delta T_{lift}} \tag{9}$$

$$COP_{HP,H} = \eta_{rec}.\frac{T_{cond}}{\Delta T_{lift}} \tag{10}$$

where η_{rec} is the Carnot efficiency of the reciprocating prototype, modelled as a function of the temperature lift. Based on the experimental analysis of Gasser et al. [6], the Carnot efficiency is captured with the following piecewise-linear correlation:

$$\eta_{rec} = \begin{cases} 0.50, & \Delta T_{lift} \leq 10K \\ 0.50 + 0.01(\Delta T_{lift} - 10), & 10K < \Delta T_{lift} < 20K \\ 0.60, & \Delta T_{lift} \geq 20K \end{cases} \tag{11}$$

The heating or cooling capacity is then obtained from the COP and the electrical power. The entire map is scaled such that at a chosen reference operating point (loop temperature and design lift) the reciprocating LHP delivers the same nominal zone capacity as the commercial LHP.

4.5.3. Low-lift turbo-compressor local heat pump

The low-lift turbo-compressor LHP archetype represents the second prototype in Gasser et al. [6], where a small oil-free radial turbo compressor uses butane (R600) as refrigerant. This machine is specifically designed for low-lift operation, with compressor aerodynamics and heat-exchanger design chosen to minimise internal losses for lifts of roughly 10 to 25 K. The experimental results show very high COPs and, more importantly, a Carnot efficiency that is both high and nearly constant over the investigated range of ΔT_{lift}:

$$COP_{HP,C} = \eta_{turbo} \cdot \frac{T_{evap}}{\Delta T_{lift}} \tag{12}$$

$$COP_{HP,H} = \eta_{turbo} \cdot \frac{T_{cond}}{\Delta T_{lift}} \tag{13}$$

where η_{turbo} is the Carnot efficiency of the turbo prototype, modelled as a simple function of the temperature lift. Based on the experimental analysis of Gasser et al. [6], the Carnot efficiency is captured with the following piecewise-linear correlation:

$$\eta_{tubo} = \begin{cases} 0.64, & \Delta T_{lift} \leq 13K \\ 0.64 + 0.003(\Delta T_{lift} - 13), & 13K < \Delta T_{lift} < 26K \\ 0.60, & \Delta T_{lift} \geq 26K \end{cases} \tag{14}$$

5. Supervisory control

The current system requires a supervisory controller to specify the variables needed to operate the CO_2 loop, including the compressor configuration, compressor speed, suction and discharge pressures, and the loop pressure. The supervisory strategy follows a temperature-bounded (TB) approach in which the CO_2 loop is no longer constrained to remain strictly two-phase. Instead, for a given loop pressure, the bulk CO_2 state is confined to a narrow band of ± 10℃ around the saturation temperature $T_{sat}(P_{loop})$. This defines maximum allowable heat exchange in the subcooled, two-phase, and superheated regions. The supervisory optimization problem can therefore be formulated as

$$\max_{\theta} COP_{system}$$

$$\textit{Subject to} \quad \begin{cases} P_{suc}, P_{dis} \in compressor \;\; envelope \\ S \in [30,75] \;\; Hz \\ fix\_on \in \{0,1\} \\ T_{min} \leq T_{loop} \leq T_{max} \end{cases} \tag{15}$$

where T_{min}, and T_{max} are the loop-temperature limits defined as ± 10℃ around $T_{sat}(P_{loop})$.

The net exchange between the loop and all LHPs is represented by a six-component vector Q collecting heating and cooling contributions in each of these regions as follows:

$$Q = [Q_{C,sub}, Q_{C,2\varphi}, Q_{C,sup}, Q_{H,sub}, Q_{H,2\varphi}, Q_{H,sup}] \tag{16}$$

where $Q_C \geq 0$ denotes heat rejected to the loop by cooling LHPs, and $Q_H \leq 0$ denotes heat extracted from the loop by heating LHPs in the subcooled (sub), two-phase (2φ), and superheated (sup) regions. To generate the control parameters, the proposed method is divided into two stages: an offline stage and an online stage. The offline stage builds a "base table" by enumerating feasible combinations of compressor setpoints and six-segment exchanges. The decision tuple is defined as follows:

$$\theta = (S, P_{suc}, P_{dis}, P_{loop}, fix\_on) \tag{17}$$

where S (Hz) is the variable-speed setpoint, P_{suc} and P_{dis} are suction and discharge pressures, and P_{loop} is the CO_2 loop pressure. Under the present assumption of negligible pressure drops in the loop, $P_{loop} = P_{suc}$ in cooling-dominant operation and $P_{loop} = P_{dis}$ in heating-dominant operation. Finally, $fix\_on \in \{0,1\}$ indicates whether the fixed-speed unit operates at 60 Hz. A discrete grid in $(S, P_{suc}, P_{dis}, P_{loop}, fix\_on)$ is swept; for each grid point within the compressor envelope, loop mass flow is obtained from the dual-compressor maps, the enthalpy bounds and the regional caps are evaluated, all admissible six-segment vectors Q (quantized in 1 kW steps and limited by the enthalpy bounds) are enumerated, and the corresponding system COP is calculated as follows:

$$COP_{system}(\theta; Q) = \frac{Q_C(Q)+|Q_H(Q)|}{\dot{W}_{HP}(\theta,Q)+\dot{W}_{comp}(\theta)} \tag{18}$$

Each combination that respects the constraints and the circulation compressor envelope is stored as a row $(Q, \theta, COP_{system})$ in the base table.

Online, the controller receives the zone command vector $u \in \{-1,0,+1\}^{n_{HP}}$ (-1 for heating/ +1 for cooling/ 0 off) and the outdoor-unit inlet water temperature ($T_{w,OU,in}$). Using an initial guess tuple $\theta^{(0)}$, the full model solves the appropriate scalar residual (cooling or heating) to obtain a feasible circulation state. The resulting single-pipe traversal yields a continuous six-segment vector Q_{model}, which is then rounded to a discrete key Q_{target}. This key is used to query the base table for all entries with $= Q_{target}$. Candidates are tested in order of decreasing stored COP: for each one, the full model is re-run to close the loop enthalpy balance within the constraints and to verify the compressor envelope and equipment limits. The first candidate that passes these checks provides the accepted tuple $(S, P_{suc}, P_{dis}, P_{loop}, fix\_on)$, which is then used to drive the circulation compressor and stored in a runtime table for analysis.

6. Results and discussion

To capture the transient behaviour of the system, the CO_2TN is implemented in TRNSYS for the case study. The system coefficient of performance (COP_{system}) is used as the metric to compare the results and is defined as follows:

$$COP_{system}(t) = \frac{\dot{Q}_{HP}(t)}{\dot{W}_{tot}(t)} \tag{19}$$

where $\dot{Q}_{HP}(t)$, denotes the total useful thermal rate provided by the LHPs at each time step and $\dot{W}_{tot}(t)$, denotes the total electrical power consumed by the RVCC and all LHPs.

Fig. 4 (left) compares the distribution of hourly COP values for the three datasets. The base case (COP_{base}) is tightly clustered around low values, with first quartile $Q_1 = 2.078$, a median of 2.232, third quartile $Q_3 = 2.278$, and a mean of 2.129, indicating that most operating points remain close to a COP of 2.2. In contrast, the reciprocating low-lift local heat pump configuration (COP_{recp}) exhibits a much wider spread and higher central tendency, with $Q_1 = 2.697$, median 4.268, $Q_3 = 4.674$, and a mean of 3.812, showing that at least half of the hours achieve COP values above about 4. Finally, the turbo-compressor low-lift LHP configuration (COP_{turbo}) further shifts the distribution towards higher efficiencies, with $Q_1 = 2.823$, median 4.440, $Q_3 = 4.908$, and a mean of 3.995. Overall, the violin plots highlight not only the increase in average COP when moving from the base case to the two local heat pump configurations, but also the slight yet consistent improvement of the turbo configuration over the reciprocating one across the entire distribution.

Fig. 4 (right) compares the annual electrical energy consumption of the CO_2TN for cooling-only and heating-only operation, partitioned between the circulation compressor $\dot{W}_{comp}$and the LHPs. The labels C and H denote cooling-only and heating-only modes, respectively. In the base configuration, the LHPs represent a considerable fraction of the total electricity use (about 38% in cooling mode and 41% in heating mode). Moreover, changes in LHP electrical demand also affect the circulation compressor consumption, because the required CO_2 mass flow (and thus compressor work) depends on the net heat exchanged between the active LHPs and the CO_2 loop. Moving from the base case to the reciprocating and turbo compressor configurations, the LHPs become more efficient; therefore, for the same imposed building load, the electricity required by the LHPs decreases, which is consistent with the lower LHP contributions observed in the figure. In cooling-only operation, a more efficient LHP draws less electrical power to meet the same cooling load, and consequently rejects less total heat to the CO_2 loop. This reduced heat rejection lowers the mass-flow requirement for maintaining the loop operating conditions, leading to a decrease in circulation compressor energy. In heating-only operation, the trend is reversed for the compressor: for a fixed heating load, improving the LHP efficiency reduces the electrical input, which increases the portion of heat that must be absorbed from the CO_2 loop. As a result, the circulation system must transport slightly more heat through the loop, which increases the required CO_2 mass flow and yields a modest increase in circulation compressor energy. Despite this increase, the total annual energy consumption in heating-only operation still decreases because the reduction in LHP electricity dominates.

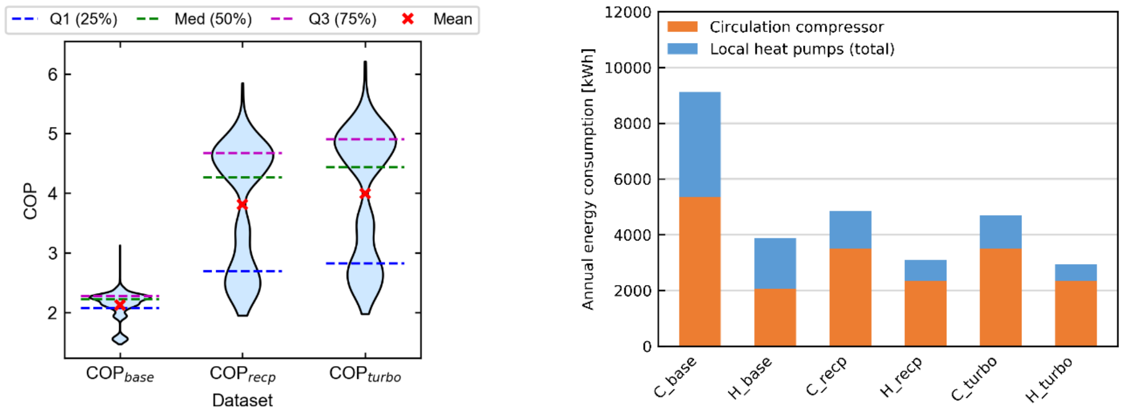

Figure 4. Violin plots of hourly COP (left) and total energy consumption (right)

To delve deeper into the shape of the violin plots in Fig. 4, we focus on the turbo-compressor results. The operating hours are separated according to whether the system is in heating- or cooling-dominant mode, and COP violin plots are drawn for each mode (Fig. 5). Fig. 5 shows that COP values in cooling mode are systematically higher and less dispersed than in heating mode, which explains the shape of the total COP distribution observed in Fig. 4. This behavior arises from the design points of the turbo-compressor LHPs in heating and cooling modes and from the design and operating envelope of the RVCC components, which are more favourable under cooling-dominant conditions.

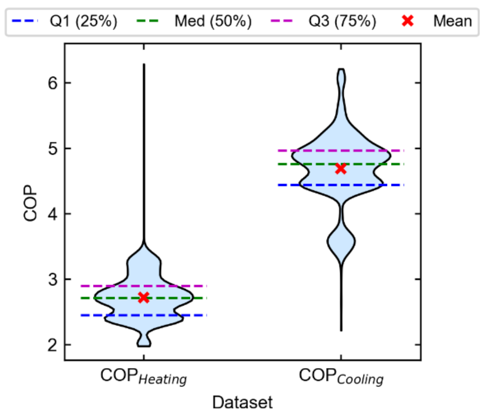

Figure 5. Violin plots of COP in heating-dominant and cooling-dominant for the turbo-compressor case

7. Conclusions

This work examined how the characteristics of local heat pumps influence the overall performance of a CO_2-based thermal network supplying year-round heating and cooling to a five-zone office building. Using a component-based model of the system integrated with a new supervisory control strategy, heating and cooling demand of an office building in Montreal were simulated for three LHP archetypes: a commercially available unit, and two heat pumps specifically designed for low-lift applications.

Results show that the choice of local heat pump designed for low-lift applications has a decisive impact on system efficiency. With the commercial LHPs, the system COP distribution is narrowly clustered around low values, with most operating hours near COP ≈ 2.2. Replacing the commercial units with low-lift heat pumps approximately doubles the typical COP, shifting the median COP to above 4 for both low-lift configurations and substantially broadening the high-performance tail. The turbo-compressor archetype provides a further, albeit more modest, improvement over the reciprocating concept, with slightly higher median and mean COP and a larger fraction of hours operating at the highest COP levels.

Overall, the study confirms that the benefits of a CO_2 thermal network cannot be fully realized with conventional heat pumps designed for large temperature lifts. Low-lift LHPs that maintain high Carnot efficiency over 10 to 30 K lifts enable much higher system-level COPs under the same plant and control constraints. From a design standpoint, the primary step change in performance arises from adopting any suitably optimized low-lift LHP; the incremental advantage of turbo- over reciprocating-based designs must then be weighed against differences in cost, complexity, and reliability.

Nomenclature

COP	Coefficient of Performance	$\dot{W}$	Electrical power (W)
H	Per-bore depth of borehole (m)	η	Carnot efficiency
h	Enthalpy (kJ×kg^{-1})	**Subscripts**	
L	Total borehole length (m)	C	Cooling
$\dot{m}$	Mass flow rate (kg×hr^{-1})	comp	Circulation compressor
N_{bx}	Number of boreholes in x-direction	dis	Discharge
N_{by}	Number of boreholes in y-direction	H	Heating
P	Pressure (MPa)	HP	Heat pump
$\dot{Q}$	Heat transfer rate (W)	loop	CO_2 loop
S	Compressor speed (Hz)	suc	Suction
T	Temperature (K or ℃)	tot	total

Acknowledgements

The authors acknowledge the Natural Sciences and Engineering Research Council of Canada (NSERC) for funding the Ph.D. student contributing to this work through discovery grant. [Funding application number: RGPIN-2020-06556]

References

[1] Eslami-Nejad P, Bastani A, Giguere D. Single-pipe thermal energy system. U.S. Patent;2023.
[2] Bastani A, Gholamrezaie S. CO2 thermal network prototype: Identifying control parameters for optimal operation in transcritical mode. *Energy Conversion and Management*, 2024;**322**:119170.
[3] Gholamrezaie S, Cimmino M, Eslami-Nejad P. Modeling and experimental validation of a single-pipe CO2 thermal network connected to local heat pumps. *Applied Thermal Engineering* 2025;**280**:128363.
[4] Gholamrezaie S, Cimmino M, and Eslami-Nejad P. Simulation and Control Strategy of a CO2 Loop for Building Thermal Management in Heating Mode. in 15th IIR-Gustav Lorentzen conference on Natural Refrigerants; 2022.
[5] Gholamrezaie S, Cimmino M, and Eslami-Nejad P. Investigating control parameters of a CO2-based thermal network connecting decentralized heat pumps. in 16th IIR-Gustav Lorentzen conference on Natural Refrigerants; 2024.
[6] Gasser L, Flück S, Kleingries M, Meier C, Bätschmann B, Wellig B. High efficiency heat pumps for low temperature lift applications. in Proceedings of the 12th IEA Heat Pump Conference; 2017.
[7] Tamasauskas J, Kegel M, and Blake J. The Potential of Heat Pump Technologies for the Replacement of Rooftop Units in Small Commercial Buildings in eSim 2018 conference.
[8] Cimmino M and Eslami-Nejad P. A simulation model for solar assisted shallow ground heat exchangers in series arrangement. *Energy and Buildings*, 2017;**157**:227-246.
[9] Badache M, Eslami-Nejad P, Ouzzane M, Aidoun Z, Lamarche L. A new modeling approach for improved ground temperature profile determination. *Renewable Energy*, 2016;**85**:436-444.
[10]Ahmadfard, M and Bernier M. A review of vertical ground heat exchanger sizing tools including an inter-model comparison. *Renewable and Sustainable Energy Reviews*, 2019;**110**:247-265.